Electronic Supplemental Information

Plasmonic heterostructure Bi_2S_3/Ti_3C_2 with continuous photoelectron injection mediated near-infrared self-powered photoelectrochemical sensing

Ding Jiang,[a] Yude Zhang,[a] Xiaojiao Du,[b] Linhua Zhang,[a] Xueling Shan,[a] Wenchang Wang,[a] Hiroshi Shiigi,[c] Zhidong Chen[a*]

[a] *Jiangsu Key Laboratory of Advanced Catalytic Materials and Technology, School of Petrochemical Engineering, Changzhou University, Changzhou, Jiangsu, 213164, P. R. China*

[b] *Oakland International Associated Laboratory, School of Photoelectric Engineering, Changzhou Institute of Technology, Changzhou, Jiangsu, 213032, P. R. China*

[c] *Department of Applied Chemistry, Osaka Prefecture University, 1-2 Gakuen, Naka, Sakai, Osaka 599-8570, Japan.*

∗Corresponding author.

Tel: +86 519 86330239

E-mail address: zdchen@cczu.edu.cn (Z. Chen)

Experimental section

Materials and reagents.

Dimethylformamide (DMF), cupric chloride ($CuCl_2$), sodium sulfide (Na_2S), bismuth nitrate pentahydrate ($Bi(NO_3)_3 \cdot 5H_2O$), sodium hydroxide (NaOH), chitosan (CTS) and ethanol were purchased from Sinopharm Chemical Reagent Co., Ltd. Titanium carbide (Ti_3C_2) was obtained from Foshan Xinxi Technology Co., Ltd. The MC-RR was achieved from Enzo Life Sciences, Inc. and its aptamer was gained from Sangon Biotech Co., Ltd., with the following sequence: 5'- CAG CTC AGA AGC TTG ATC CTA CTG CCC TTC AAT GTT CAC TCC TGT TTC CTG ATC TTT GTC GAC TCG AAG TCG TGC ATC TG -3'.[1] All the aqueous solution involved was prepared with ultrapure water (18.2 MΩ cm^{-1}).

Preparation of the Bi_2S_3 and Bi_2S_3/Ti_3C_2 heterojunction.

To prepare the Bi_2S_3/Ti_3C_2 heterojunction, 538 mg of weighted $Bi(NO_3)_3 \cdot 5H_2O$ was dissolved in 50 mL dilute nitric acid (0.5 M) under continuous magnetic stirring control. Then, the above solution was dropwise added into 30 mL of Ti_3C_2 dispersion (0.5 mg/mL) and kept in ultrasonic treatment for several minutes, the mixed solution was marked as solution A. Meanwhile, 398.7 mg of Na_2S was dissolved in 50 mL of water, which was named as solution B. Subsequently, the solution B was slowly added into the solution A under vigorous stirring until a black-brown precipitate was observed. Furthermore, the black-brown precipitate was freeze-dried to remove the moisture and as such, the Bi_2S_3/Ti_3C_2 heterojunction were acquired for use. Besides, the Bi_2S_3 was prepared in a similar process without the addition of Ti_3C_2.[2]

Preparation of CuO.

CuO nanomaterials were prepared according to previous method with slight modification.[3] Firstly, 4 mM $CuCl_2$ was dissolved in 20 mL of water. Then, 0.1 M of NaOH was gradually added to adjust the pH value of the solution to 10 under vigorous stirring. After that, the mixed solution was then transferred into the Teflon

lined stainless steel reactor and kept at 150 °C for 12 h. After cooling down, the obtained product was centrifuged at 8000 rpm for 12 min and washed with water for several times. The precipitate was then dried at 75 °C overnight for further use.

Construction of self-powered aptasensors.

Prior to modification, the ITO electrodes were placed in ultrasonic cleaning machine with acetone, ethanol, and distilled water for ten minutes, respectively, and then dried under nitrogen gas flow. The Bi_2S_3/Ti_3C_2 heterojunction and CuO powder were dispersed in DMF to obtain 10 mg/mL suspension. Subsequently, by fixing a modified area of 0.5 cm × 1 cm, 20 μL of the obtained Bi_2S_3/Ti_3C_2 and CuO suspensions were modified on the conductive surface of the ITO electrodes, respectively. These electrodes were marked as Bi_2S_3/Ti_3C_2/ITO and CuO/ITO, and then dried at 60 °C oven for 8 hours. After cooling down to room temperature, the CuO/ITO electrodes were fixed with 10 μL chitosan (CTS, 5 mg/mL). Twenty microliters of the MC-RR aptamer (2.5 μM) was coated on CTS/CuO/ITO and incubated at room temperature for several hours to prepare Apt/CTS/CuO/ITO. To remove redundant aptamers, the obtained Apt/CTS/CuO/ITO modified electrodes were rinsed with 0.1 M phosphate buffer solution (PBS, pH = 7.4) for several times. The digital photos of the whole equipment of the dual-photoelectrode-based self-powered sensor were shown in Fig. S1.

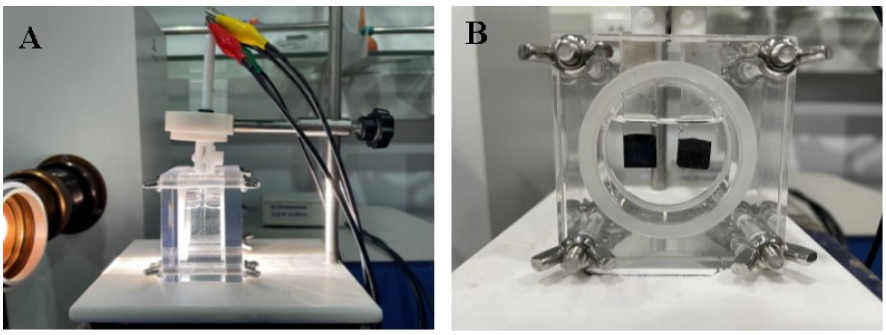

Fig. S1 Digital photos of the whole equipment of the dual-photoelectrode-based self-powered sensor.

Sensitive detection of MC-RR.

To construct a dual-photoelectrode based self-powered sensor, the Bi_2S_3/Ti_3C_2/ITO was used as photoanode, and Apt/CTS/CuO/ITO modified electrodes acted as photocathode, respectively. Prior to starting the detection, a certain concentration of MC-RR was incubated with the Apt/CTS/CuO/ITO for 30 minutes to realize the interaction between MC-RR and the modified electrodes. After rinsing with 0.1 M phosphate buffer solution (PBS, pH = 7.4), the dual-photoelectrode system was used to collect signals of the self-powered sensor in PBS (0.1 M, pH = 7.4).

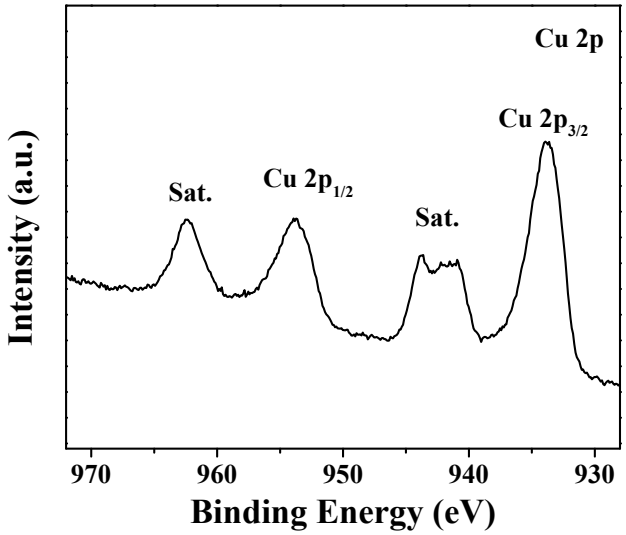

Fig. S2 The XPS high-resolution spectra of Cu 2p.

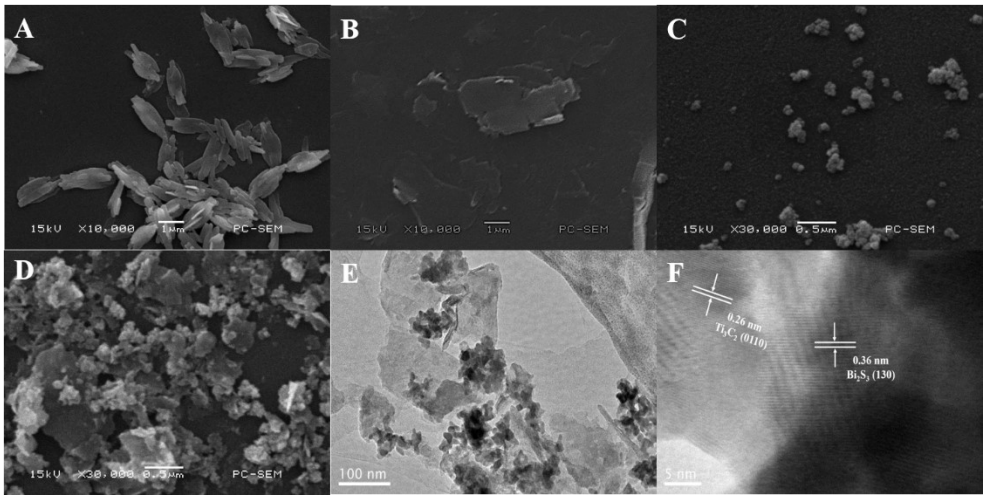

Fig. S3 SEM image of the (A) CuO; (B) Ti_3C_2; (C) Bi_2S_3 and (D) Bi_2S_3/Ti_3C_2. (E) TEM image and (F) HRTEM of the Bi_2S_3/Ti_3C_2 heterojunction.

As shown in Fig. S3A, the obtained CuO had a typical shrimp head structure with the size of about 3 μm, which was similar to the previous article.[4] Ti_3C_2 MXene showed a broad sheet-like morphology (Fig. S3B), while pure Bi_2S_3 showed a sphere structure (Fig. S3C).[5] In the Bi_2S_3/Ti_3C_2 heterojunction, Bi_2S_3 nanoparticles were distributed on the surface of two-dimensional sheet-like Ti_3C_2 (Fig. S3D). To further study the morphology of the Bi_2S_3/Ti_3C_2 heterojunction, the TEM test was implemented. As shown in Fig. S3E, Bi_2S_3 clusters were well-distributed on lamellar plasmonic Ti_3C_2 nanosheets, which was in consistent with the SEM results. Fig. S3F displayed the HRTEM image of the Bi_2S_3/Ti_3C_2 heterojunction. Obviously, the lattice spacing of 0.26 nm and 0.36 nm were observed, which were in good agreement with the (0110) planes of Ti_3C_2 and (130) planes of Bi_2S_3, respectively.[6]

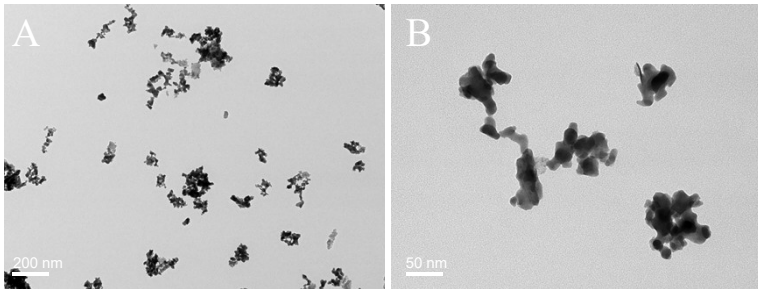

Fig. S4 TEM images of pure Bi_2S_3 nanoparticles.

The TEM images of Bi_2S_3 have been measured in Fig. S4. As can be seen, pure Bi_2S_3 nanoparticles (NPs) tended to aggregate.

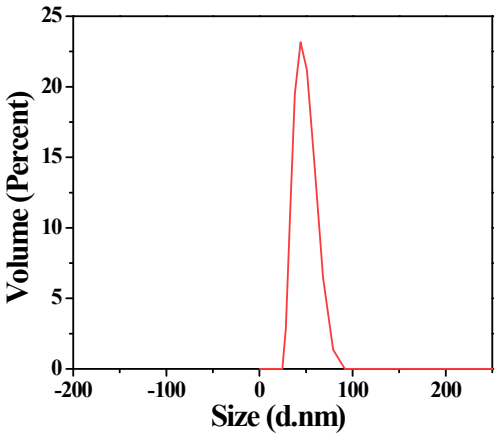

Fig. S5 DLS spectrum of pure Bi_2S_3 nanoparticles.

Moreover, DLS spectrum of pure Bi_2S_3 nanoparticles indicated that the Bi_2S_3 NPs ranged from 20 to 85 nm.

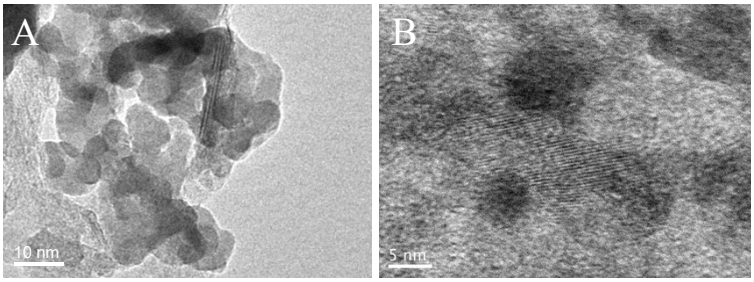

Fig. S6 HRTEM images of Bi_2S_3/Ti_3C_2 heterostructure.

In order to further confirm the state of Bi_2S_3 in the Bi_2S_3/Ti_3C_2 heterostructure, HRTEM images have been investigated in Fig. S6. Obviously, Bi_2S_3 NPs with the size of 5~10 nm were decorated on the surface of Ti_3C_2 MXene sheets. All these results proved the successful synthesis of the Bi_2S_3/Ti_3C_2 heterojunction.

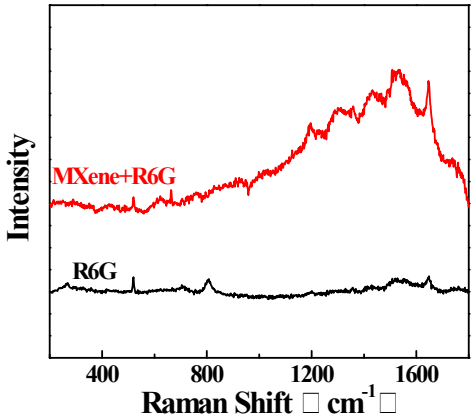

Fig. S7 SERS enhancement (514 nm excitation) of Rhodamine 6G on $Ti_3C_2T_x$ MXene substrates and Si substrate.

Surface-enhanced Raman spectroscopy (SERS) is a promising technique for identification of small quantities of molecules due to its highly efficient, noninvasive and versatile nature. SERS substrates rely primarily on plasmonic effects in electromagnetic "hot-spots" and highly concentrated charges originating from surface roughness.[7] Thus, in this work, SERS was used to prove the plasmonic effect of MXene. As can be seen in Fig. S7, we have demonstrated a large Raman signal enhancement of organic dyes on the surface of 2D $Ti_3C_2T_x$ MXene, with detection of Rhodamine 6G (R6G) at 10^{-7} M concentration using 514 nm lasers. This result indicated the plasmonic effect of MXene.

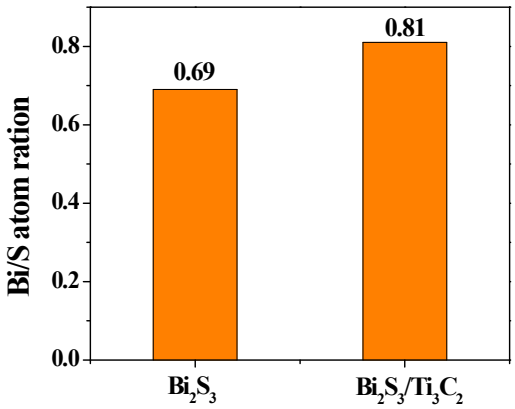

Fig. S8 The Bi/S atom ratios in pure Bi_2S_3 and Bi_2S_3/Ti_3C_2 composites.

XPS was applied to investigate the atomic ratios to find out their vacancy type. The Bi/S atomic ratios of the Bi_2S_3 and Bi_2S_3/Ti_3C_2 samples was presented in Fig. S8. The Bi/S atomic ratio of pure Bi_2S_3 is close to the theoretical value, suggesting no or relatively little element vacancy. Moreover, the Bi/S atomic ratio of Bi_2S_3/Ti_3C_2 samples is 0.81, confirming the existence of sulphur vacancies inside the Bi_2S_3/Ti_3C_2 nanocomposotes.[8,9]

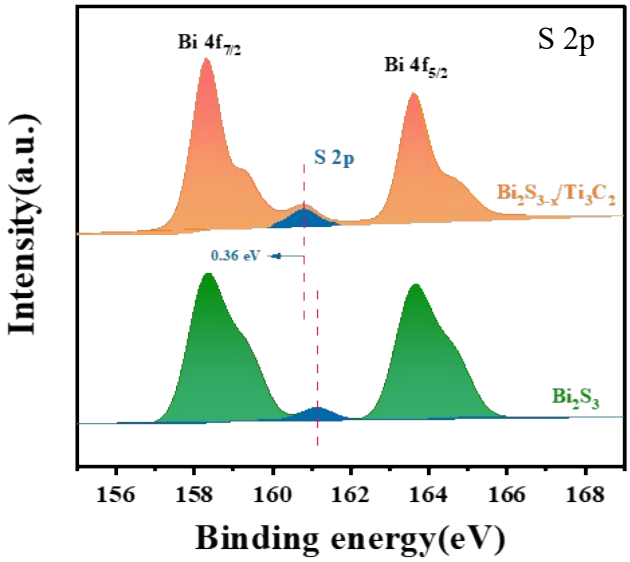

Fig. S9 The XPS high-resolution spectra of S 2p in pure Bi_2S_3 and Bi_2S_3/Ti_3C_2 composites.

As can be seen in Fig. S9, the small peak at ~160.8 eV corresponds to S 2p of pure Bi_2S_3. Compared to pure Bi_2S_3, The S 2p peak of Bi_2S_3/Ti_3C_2 composite move to relatively lower binding energies with an energy shift of 0.36 eV, indicating the reduced S 2p valence state and successful incorporation of sulfur vacancies in the Bi_2S_3/Ti_3C_2 composite.[9,10]

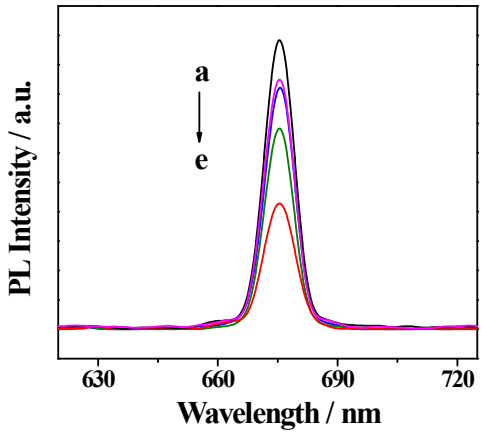

Fig. S10 Photoluminescence spectra of different samples: Bi_2S_3 (a), Bi_2S_3/20%Ti_3C_2 (b), Bi_2S_3/10%Ti_3C_2 (c), Bi_2S_3/5%Ti_3C_2 (d), and Bi_2S_3/3%Ti_3C_2 (e).

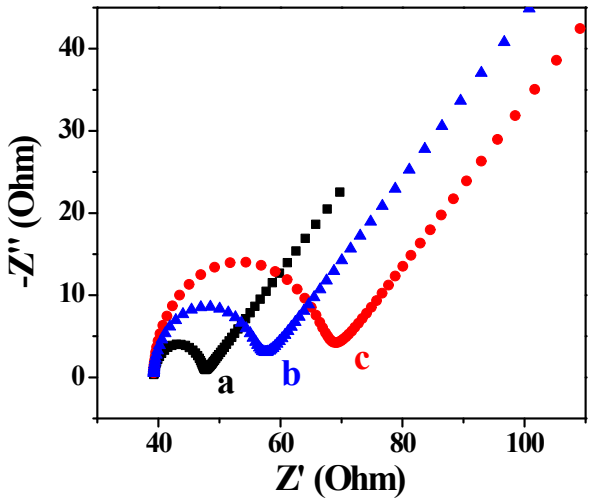

Fig. S11 EIS spectra of (a) Bi_2S_3/Ti_3C_2, (b) Ti_3C_2 and (c) Bi_2S_3.

In Fig. S11, after the integration of Bi_2S_3 and Ti_3C_2 MXene, it displayed the lowest R_{et} value. These might be attributed to the excellent electrical conductivity of Ti_3C_2 which was beneficial for the transfer of electrons.[11]

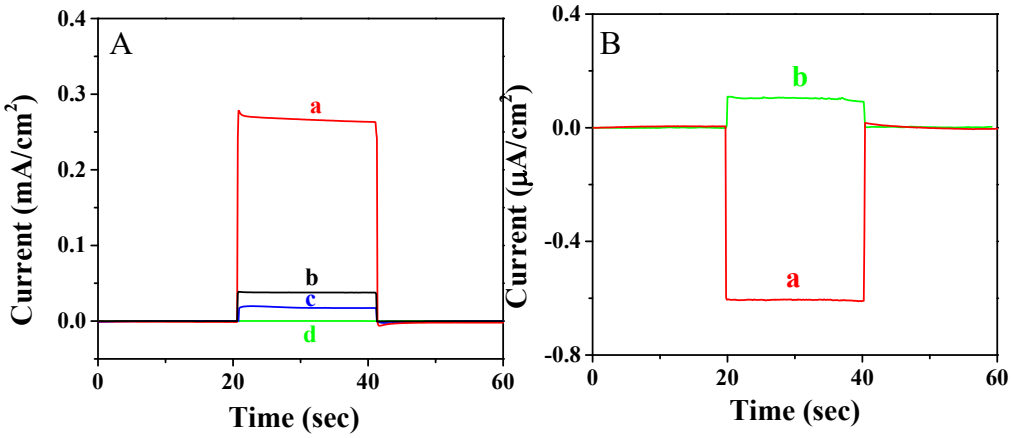

Fig. S12 (A) Photocurrent responses of photoanode: (a) Bi_2S_3/Ti_3C_2, (b) Bi_2S_3, (c) Ti_3C_2, and (d) ITO; (B) Photocurrent responses of photoanode: (a) CTS/CuO/ITO and (b) ITO.

Fig. S12A presented that the Bi_2S_3/Ti_3C_2 heterojunction possessed an enhanced current about 0.2667 mA/cm^2, which was 7.06-fold and 15.17-fold intensity of pure Bi_2S_3 and Ti_3C_c, respectively. These might be attributed to the plasmonic Ti_3C_2 could promote the generation of hot electrons and the presence of sulfur vacancies could increase more active sites and accelerate electron transfer as well.[12] Meanwhile, the photocurrent density of photocathode CTS/CuO/ITO was shown in Fig. S12B, which displayed the opposite direction of photoanode photocurrent responses, and kept at a value of 0.6029 μA/cm^2. The integration of the n-type photoanode and p-type photocathode could enable the photoanode electrons can flow to the photocathode holes through external circuit driven by inherent bias between the Fermi levels (EF) of the two photoelectrodes.

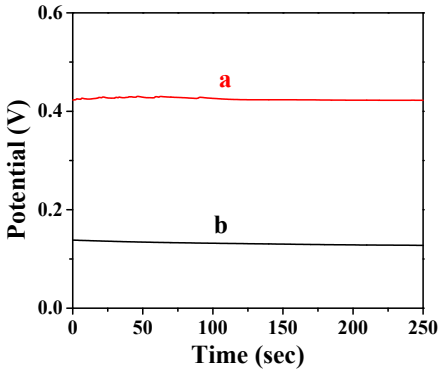

Fig. S13 OCP of the designed self-powered sensor (a) with and (b) without the simulated irradiation.

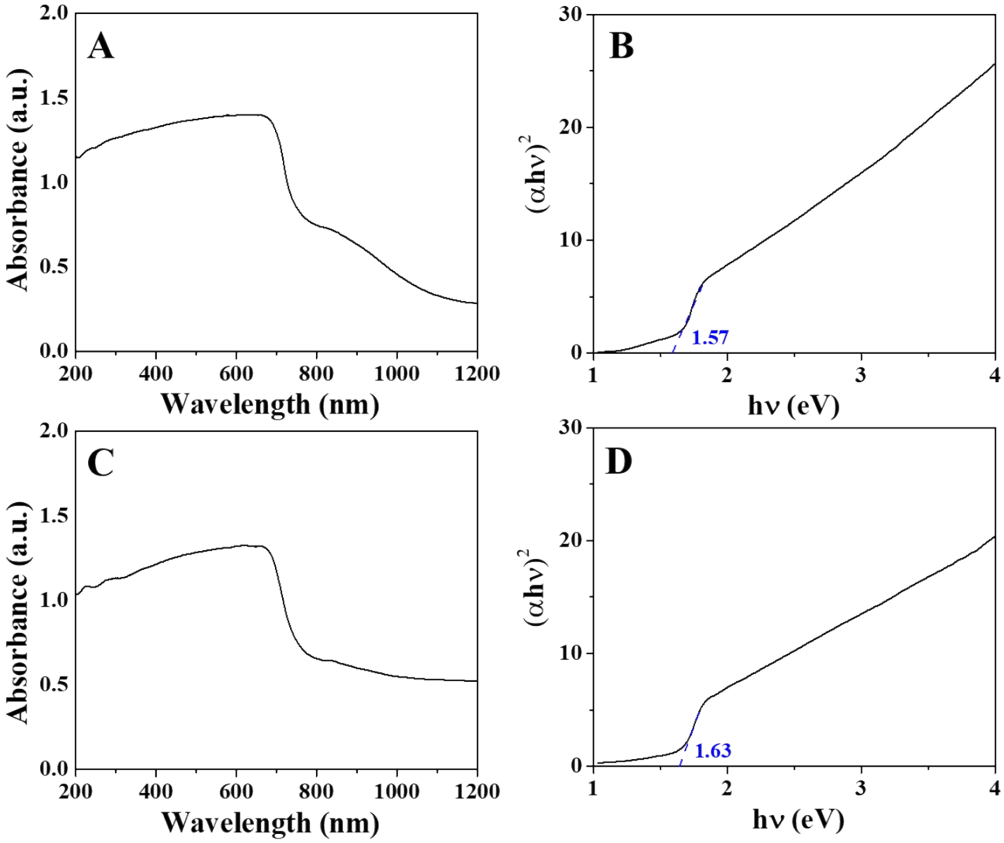

Fig. S14 UV-vis diffuse reflectance spectra of (A) Bi_2S_3/Ti_3C_2 heterojunction and (C) CuO; Plots of $(\alpha h\upsilon)^2$ versus the energy ($h\upsilon$) for the band gap energy of (B) Bi_2S_3/Ti_3C_2 heterojunction and (D) CuO.

According to the intercept of the plots of $(\alpha h\nu)^2$ vs. photon energy (Fig. S14), the bandgap (E_g) of the sulfur-defect Bi_2S_3/Ti_3C_2 heterojunction and CuO was calculated about 1.57 eV and 1.63 eV, respectively.

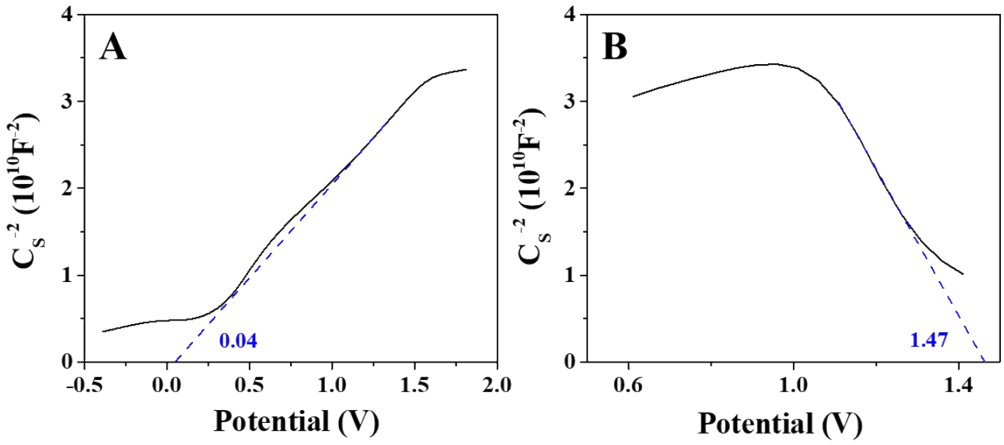

Fig. S15 The Mott-Schottky plots of (A) Bi_2S_3/Ti_3C_2 heterojunction and (C) CuO.

Mott-Schottky plots were measured to further analyze the band structure of the Bi_2S_3/Ti_3C_2 heterojunction and CuO. The Bi_2S_3/Ti_3C_2 heterojunction (Fig. S15A) showed positive slope of the line fitted, which was in accordance with the characteristic of the typical n-type semiconductor. On the contrary, the negative slope indicated that CuO was a p-type semiconductor **(**Fig. S15B**)**. In addition, the flat band potential (V_{fb}) can be calculated as the linear intercept of the horizontal axis, and the flat band potential is nearly the CB for the n-type semiconductor while the flat band potential is approximate to the VB for the p-type semiconductor. At this point, the CB of n-type semiconductor Bi_2S_3/Ti_3C_2 heterojunction was 0.04 eV and the VB of p-type semiconductor CuO was 1.47 eV, respectively. Afterwards, the VB edge of the Bi_2S_3/Ti_3C_2 heterojunction and the CB edge of CuO could be calculated as 1.61 eV and –0.16 eV with the formula $E_g = E_{VB} - E_{CB}$.[13]

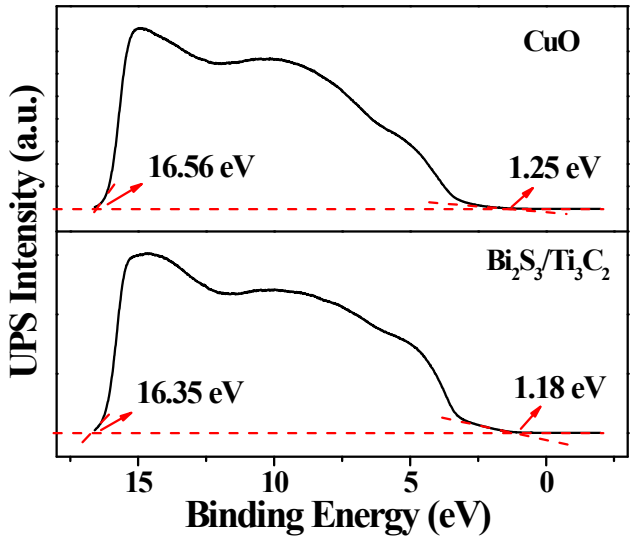

Fig. S16 UPS spectra of the CuO and Bi_2S_3/Ti_3C_2 nanocomposites.

The UPS of Bi_2S_3/Ti_3C_2 and CuO should be added to confirm the position of their VB. The secondary-electron cut-off and valence-band regions of Bi_2S_3/Ti_3C_2 and CuO were shown in Fig. S16, respectively. The valence band (VB vs vacuum) could be obtained according to the following Eq. :[14-16]

$$E_{VB} = h\upsilon - E_{cut\text{-}off} - E_H$$

where $h\upsilon$ is a constant of 21.22 eV (incident photon energy from the He I light source), $E_{cut\text{-}off}$ is the cut-off energy and E_H is energy gap between the valence band position.[15,16] The valence bands of Bi_2S_3/Ti_3C_2 and CuO were calculated to be 6.05 eV and 5.91 eV (vs vacuum). Thus, the E_{VB} values of Bi_2S_3/Ti_3C_2 and CuO are calculated to be 1.61 eV and 1.47 eV (vs reversible hydrogen electrode (RHE)), which is consistent with Mott-Schottky plots.

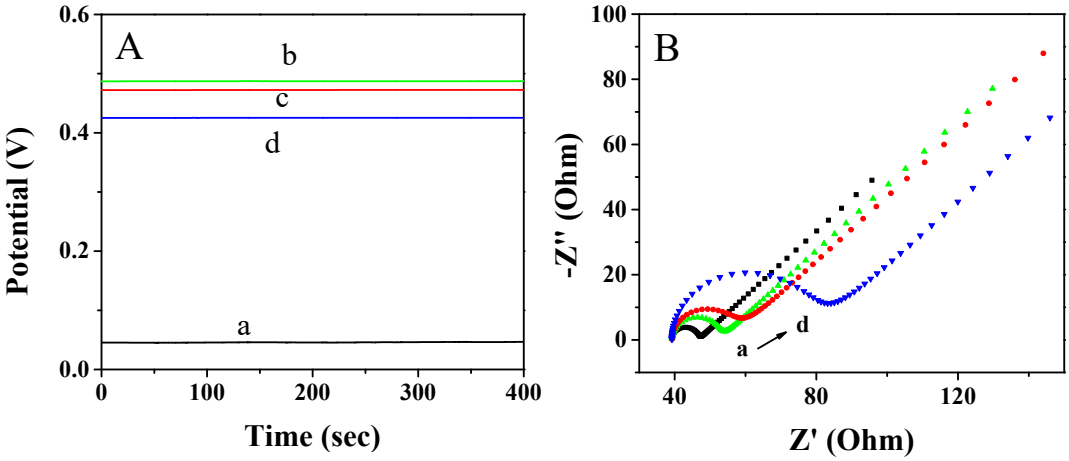

Fig. S17 (A) Chronopotentiometry and (B) EIS of the self-powered aptasensor fabrication process: (a) bare ITO, (b) CTS/CuO/ITO, (c) Apt/CTS/CuO/ITO and (d) MC-RR interacted with the Apt/CTS/CuO/ITO.

The Bi_2S_3/Ti_3C_2 heterojunction acted as photoanode material in the whole experiment, which owned the advantages of perfect conductivity of layered Ti_3C_2 and great optical performance of Bi_2S_3. As shown in Fig. S17A, when CTS/CuO/ITO was used as photocathode, the potential was about 0.49 V (curve b). After the CTS/CuO/ITO was incubated with the MC-RR aptamer, the process of electron transfer was impeded and a lower potential about 0.47 V (curve c) was obtained. In the presence of MC-RR, the target could combine well with the aptamer, further enlarging the steric hindrance, and resulting a reduced potential (0.43 V) (curve d).[17] The EIS (Fig. 3D) could also account for the feasibility and stepwise fabrication process of the sensor. The CTS/CuO/ITO had a small resistance about 15 Ω (curve b), when it was further attached with MC-RR aptamer, the resistance became a larger value (20 Ω, curve c) due to the repulsion between the negative aptamer and the negative $[Fe(CN)_6]^{3-/4-}$.[18] After adding target MC-RR, it could be recognized by its aptamer, and then the impedance value increased to 44 Ω (curve c) due to the growing steric hindrance, which blocked the transfer of electron, resulting the decreased OCP value. The EIS data (Fig. S17B) was quite consistent with the results of chronopotentiometry curves, confirming the successful construction of the self-

powered sensor.

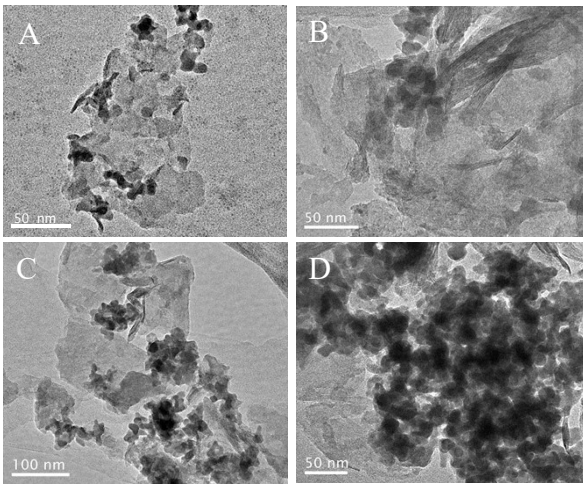

Fig. S18 TEM images of Bi_2S_3/Ti_3C_2 heterostructure with different proportions of Ti_3C_2 MXene (A) 20% ; (B) 10% ; (C) 5% ; (D) 3%.

Fig. S18 presented the TEM images of Bi_2S_3/Ti_3C_2 photocathode with different proportion of Ti_3C_2 MXene. It is obvious that the Bi_2S_3 displayed a good dispersion on Ti_3C_2 MXene as the proportion of Ti_3C_2 MXene increased.

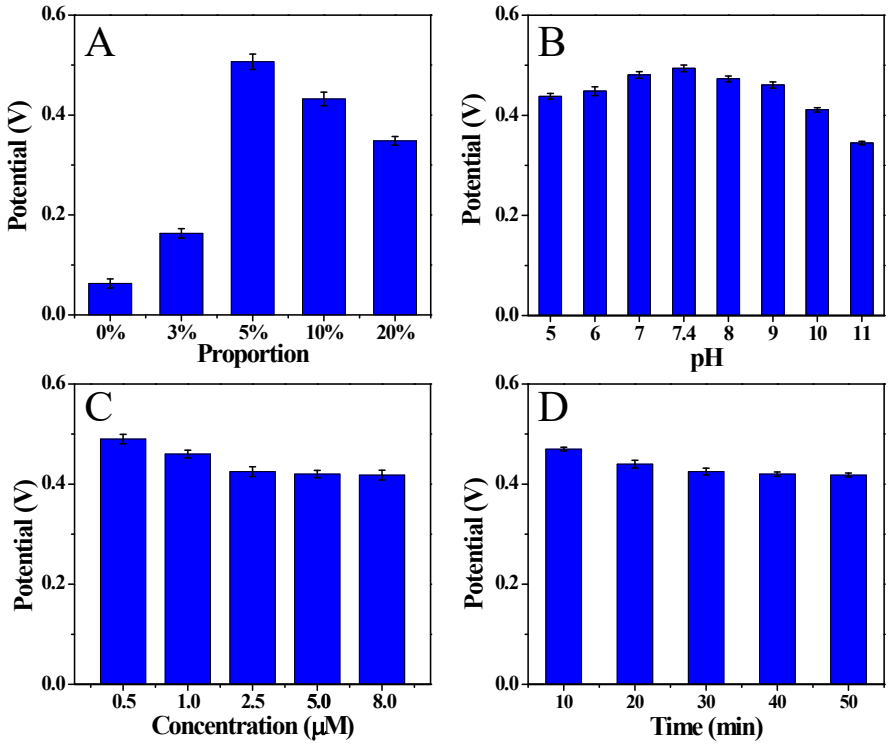

Fig. S19 The effect of (A) Ti_3C_2 proportion, (B) pH, (C) aptamer concentration and (D) incubation time on PEC sensor response.

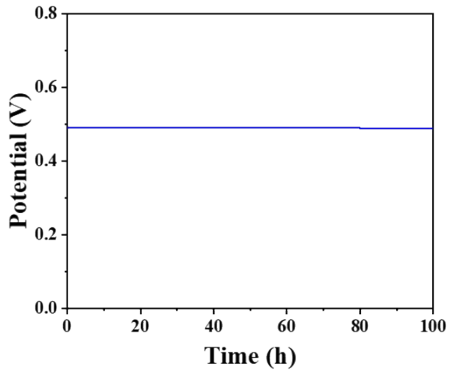

Fig. S20 Long-time stability test for self-powered aptasensor.

Fig. S20 presented the long-time OCP test of proposed sensor in 100 h. As can be seen, the proposed sensor retained about 98.9% of its initial response, suggesting that the sensor has a satisfactory long-term stability.

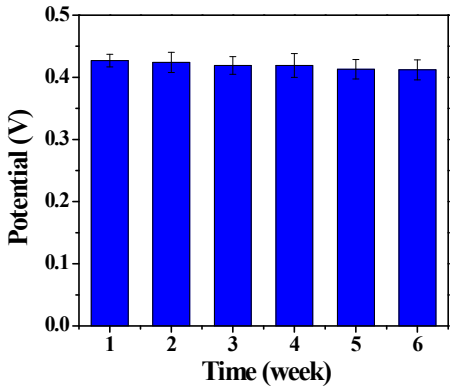

Fig. S21 Stability of the self-powered sensor after long-term storage for six weeks.

In order to evaluate the long-term stability of the sensor, the OCP of the as-fabricated sensor was measured for 6 weeks with an interval of 7 days. When it was not measured, the electrode could be washed with water and dried at room temperature, and then it was stored at 4 ^{o}C in refrigerator. As shown in Fig. S21, the proposed biosensor retained about 96.1% of its initial response after six weeks, suggesting that the as-fabricated sensor has a good stability.

Table S1. Comparison of different methods to measure MC-RR

Method	Linear range (M)	Detection limit(M)	Ref.
HPLC-MS/MS	4.8×10^{-7}-3.0×10^{-6}	9.6×10^{-8}	19
Chemiluminescence aptasensor	1.0×10^{-10}-7.0×10^{-7}	3.2×10^{-11}	20
Fluorescence biosensor	1.0×10^{-14}-0.3×10^{-8}	3.0×10^{-10}	21
SERS Detection	1.0×10^{-12}-5.0×10^{-7}	0.8×10^{-12}	1
PEC aptasensor	1.0×10^{-16}-1.0×10^{-11}	4.7×10^{-17}	This work

Table S2. Real samples detection based on the as-fabricated self-powered aptasensor.

Sample	Added (pM)	Detected (pM)	Recovery (%)	RSD (%) (n=3)
Tap water	0	-	-	-
	0.5	0.52	104.0	2.2
	1.0	0.97	97.0	4.2
Pond water	0	-	-	-
	0.5	0.49	98.0	4.5
	1.0	1.04	104.0	5.8
Fish sample	0	-	-	-
	0.5	0.51	102.0	5.3
	1.0	0.99	99.0	6.4

References

1. X. J. Luo, X. J. Zhao, G. Q. Wallace, M. H. Brunet, K. J. Wilkinson, P. Wu, C. X. Cai, C. G. Bazuin and J. F. Masson, *ACS Appl. Mater. Inter.*, 2021, **13**, 6545-6556.

2. Q. J. Yang, W. Gao, W. Zhong, M. Tao, Y. R. Qi, S. J. Bao and M. W. Xu, *New J. Chem.*, 2020, **44**, 3072-3077.

3. W. A. El-Said, M. A. AlMalki, E. M. Sayed, D. A. El-Hady and W. Alshitari, *Mater. Lett.*, 2020, **279**, 128498.

4. E. Yao, N. Zhao, Z. Qin, H. Ma, H. Li, S. Xu, T. An, J. Yi and F Zhao, *Nanomaterials*, 2020, **10**, 725.

5. Y. Liu, H. Zeng, Y. Chai, R. Yuan and H. Liu, *Chem. Commun.*, 2019, **55**, 13729-13732.

6. J. Li, Z. Li, X. Liu, C. Li, Y. Zheng, K. Yeung, Z. Cui, Y. Liang, S. Zhu, W. Hu, Y. Qi, T. Zhang, X. Wang and S. Wu, *Nat. Commun.*, 2021, **12**, 1-10.

7. A. Sarycheva, T. Makaryan, K. Maleski, E. Satheeshkumar, A. Melikyan, H. Minassian, M. Yoshimura and Y. Gogotsi, *J. Phys. Chem. C*, **2017**, 121, 19983-19988

8. H. L. Sun, Z. F. Jiang, D. Wu, L. Q. Ye, T. Q. Wang, B. Wang, T. C. An and P. K. Wong, *ChemSusChem*, 2019, **12**, 890-897.

9. Y. J. Luo, P. Shen, X. C. Li, Y. L. Guo and K Chu, *Nano Res.*, 2022, **15**, 3991-3999.

10. W. Zong, F. L. Lai, G. J. He, J. R. Feng, W. Wang, R. Q. Lian, Y. E. Miao, G. C. Wang, I. P. Parkin and T. X. Liu, *Small*, 2018, **14**, 1801562.

11. W. Zong, F. Lai, G. He, J. Feng, W. Wang, R. Lian, Y. Miao, G. Wang, I. Parkin and T. Liu, *Small*, 2018, **14**, 1801562.

12. B. Chang, Y. Guo, D. Wu, L. Li, B. Yang and J. Wang, *Chem. Sci.*, 2021, **12**, 11213-11224.

13. M. Zhang, Z. Zhang, Y. Xu, Z. Wen, C. Ding, Y. Guo and K. Wang, *Biosens. Bioelectron.*, 2020, **156**, 112135.

14. 1. M. Li, H. S. Yao, S. Y. Yao, G. Chen and J. X. Sun, *J. Colloid Interface Sci.*, 2023, **630**, 224-234.

15. L. J. Gao, L. Chen, J. T. Ren, C. C. Weng, W. W. Tian and Z. Y. Yuan, *J. Colloid Interface Sci.*, 2021, **589**, 25-33.

16. C. Y. Chu and M. H. Huang, *J. Mater. Chem. A*, 2017, **5**, 15116-15123.

17. D. Jiang, X. Du, L. Zhou, H. Li and K. Wang, *Anal. Chem.*, 2017, **89**, 4525-4531.

18. X. Ouyang, L. Tang, C. Feng, B. Peng, Y. Liu, X. Ren, X. Zhu, J. Tan and X. Hu, *Biosens. Bioelectron.*, 2020, **164**, 112328.

19. X. Y. Xu, B. Q. Zhu, Z. Liu, F. Wang and J. J. Liang, *J Chromatogr B*, 2019, **1125**, 121709.

20. B. R. Liu, X. H. Li, S. M. Liu and X. Hun, *Microchem. J.*, 2019, **145**, 648-654.

21. Y. Shi, J. Z. Wu, Y. J. Sun, Y. Zhang, Z. W. Wen, H. C. Dai, H. D. Wang and Z. Li, *Biosens. Bioelectron.*, **2012**, 38, 31-36.